Environmental Science and Pollution Research (2022) 29:29117–29129
https://doi.org/10.1007/s11356-021-18380-8

RESEARCH ARTICLE

# Removal of toluene and $SO_2$ by hierarchical porous carbons: a study on adsorption selectivity and mechanism

**Xinlei Huang[1] · Hongxian Li[1] · Ling Wang[1] · Minghui Tang[1] · Shengyong Lu[1]**

Received: 2 October 2021 / Accepted: 23 December 2021 / Published online: 7 January 2022


## Abstract

The coal combustion produces a large amount of pollutants such as organic compounds pollutants (such as VOCs, SVOCs) and conventional pollutants (such as $SO_2$, NOx) which need to be controlled in coal-fired plants. Currently, there have been mature emission control technologies for conventional pollutants in coal-combustion flue gas. The complicated conditions of flue gas will have great effects on the property of VOCs adsorbents. Thus, high-quality adsorbents with great adsorption properties and selectivity of VOCs are urgently needed. In this work, a biomass-derived hierarchical porous carbon (HPC-A) with high adsorption capacity (585 mg/g) and great selectivity of toluene was proposed. Analyses through the competitive adsorption tests between toluene and $SO_2$ indicated that the pore size distributions of adsorbents dominate the adsorption capacity and selectivity. The ultramicropores (< 0.7 nm) determine the $SO_2$ adsorption capacity and promote the $SO_2$ adsorption selectivity, while the micropores of 0.7 ~ 2 nm and mesopores are beneficial for toluene adsorption. Intriguingly, the $SO_2$ molecules can promote the toluene adsorption kinetics on hierarchical porous carbons through occupying ultramicropores when competitive adsorption. Besides, we indicated the mechanism of adsorption capacity, selectivity, and kinetics of toluene and $SO_2$, and great reusability of HPC-A was found through toluene cyclic adsorption tests. The HPC-A could be a potential adsorbent for VOCs removal from coal-combustion flue gas.

**Keywords** Toluene · $SO_2$ · Competitive adsorption · Adsorption kinetics · Hierarchical porous carbon

## Introduction

China is the largest coal producing and consuming country in the world, and the coal combustion process would produce various pollutants such as sulfur dioxide ($SO_2$), nitrogen oxides (NOx), organic pollutants (VOCs, SVOCs), and particulate matter (PM) (Wu et al. 2021a). Nowadays, the emission standards of air pollutants from coal-fired sources are increasingly strict, and the emissions of conventional pollutants (such as $SO_2$, NOx, and particulates) have been effectively reduced to very low levels especially in ultra-low emission coal-fired power plants (Tang et al. 2019a; Wu et al. 2021b). However, the organic pollutants have received little attention, and no special equipment or technology is applied to control their emissions in coal-fired plants (Ma et al. 2021). With large volume of coal-fired flue gas discharged into the environment, the coal-fired power plants become an important anthropogenic source of organic pollutants (Xu et al. 2019). The VOCs have long been a series of widely concerned toxic and harmful pollutants as most VOCs are recognized as precursors of photochemical oxidants, substances causing the acid rain, agents that destroy the ozone stratospheric layer, factors causing the climatic change, and poisons that affect the nervous system and carcinogenic and mutagenic agents (Lillo-Ródenas et al. 2005; Mohan et al. 2009). Compared with other sources, coal and industrial combustion sources accounted for a large proportion of VOCs (Cheng et al. 2021). It is crucial to take measures to reduce VOCs emission from coal-fired power plants.

For the $SO_2$ removal from coal-fired plants, there have been mature technologies such as wet flue gas desulfurization (Lim et al. 2021) and semi-dry desulfurization (Zhou et al. 2021). The flue-gas desulfurization (FGD) processes can abate at least 99% of $SO_2$ emissions to the atmosphere

Responsible Editor: Tito Roberto Cadaval Jr.

✉ Minghui Tang
lytmh1214@zju.edu.cn

[1] State Key Laboratory for Clean Energy Utilization, Institute for Thermal Power Engineering, Zhejiang University, Hangzhou 310027, China

(Rodrigues et al. 2021). However, for the VOCs removal, great efforts have been made to develop efficient, environmental friendly, and economic VOCs abatement techniques such as catalysis oxidation (Zhou et al. 2020; Tang et al. 2019b), biological degradation (Muñoz et al. 2013; Padhi and Gokhale 2014), condensation (Li et al. 2020; Wang et al. 2020), and adsorption (Zhao et al. 2018), among which adsorption with carbon adsorbents is recognized as one of the most economic and promising VOCs removal strategies (Zhang et al. 2017). As the $SO_2$ already had mature and efficient abatement techniques in coal-fired plants, the VOCs are urgent to be more effective controlled. Adsorption can be an ideal treatment strategy for VOCs, and adsorbents with high VOCs adsorption capacity and selectivity in flue gas of coal-fired plants should be proposed.

The flue gas in the coal-fired plants is multicomponent gas, and in the process of multi-components adsorption, different adsorbates have various molecular diameters and polarities, which put forward different requirements for the pore structure or surface functional groups of adsorbents (Qie et al. 2019; Deng et al. 2017; Sun et al. 2016a). For example, the dynamic diameter of $SO_2$ molecule is 0.28 nm, which is much smaller than toluene molecules (0.68 nm). Thus, the favorable pore sizes for $SO_2$ and toluene adsorptions should be distinct (Qie et al. 2019). Related research (Zhu et al. 2012) had reported that the $SO_2$ adsorption capacity was determined by the ultramicropore (< 0.7 nm) of adsorbents. For the toluene adsorption, related research (Lillo-Ródenas et al. 2005) had revealed that the toluene is mainly adsorbed in micropore of adsorbents. However, some researches (Kim and Ahn 2012; Gil et al. 2014) hold the point that the larger pores are good to the adsorption of VOCs with larger molecular diameters because of the wider transport channel provided by meso-macropores. Our previous work (Lu et al. 2021) also revealed that the meso-macropores are beneficial to the toluene adsorption kinetics and the mesopores can promote the toluene adsorption capacity to some degree. Besides, surface functional groups such as the nitrogenous functional groups (Zhang et al. 2020; Sun et al. 2016b) and the alkaline oxygen functional groups (He and He 2016; Li et al. 2011) in carbon adsorbents have definite effects for $SO_2$ and toluene adsorption.

In this work, we synthesized a serious of hierarchical porous carbons (HPCs) with different pore size distributions. Toluene, $SO_2$ single, and competitive dynamic adsorption tests were conducted on HPCs and a type of commercial activated carbon (AC) to systematically discuss the mechanism of the adsorption property. And toluene cyclic adsorption experiments were conducted on HPC-A to test its reusability. Through these tests, we proposed a hierarchical porous carbon (HPC-A) with high toluene adsorption capacity, selectivity, great toluene adsorption kinetics, and reusability. It can be an appropriate adsorbent for VOCs adsorption in multicomponent gas, especially coal-fired flue gas.

## Material and methods

### Materials

The α-cellulose (50 μm) (AR) was received from Aladdin Chemistry Co., Ltd. $(NH_4)_2C_2O_4{\cdot}H_2O$ (AR), $NaHCO_3$ (AR), $KHCO_3$ (AR), $K_2CO_3$ (AR), and toluene (AR) were purchased from Sinopharm Chemical Reagent Co., Ltd.

### Preparation of adsorbents

In this work, four kinds of carbon adsorbents were prepared from various approaches. The hierarchical porous carbons (HPCs) were synthesized in laboratory. The HPC-A and HPC-B were prepared by "foaming method" which had been applied by our previous researches (Lu et al. 2021; Tang et al. 2020). The HPC-C was prepared by the method of co-activation of α-cellulose and $K_2CO_3$. The preparation details of HPCs are described as follows.

First is thoroughly mingling α-cellulose, $(NH_4)_2C_2O_4{\cdot}H_2O$, and $KHCO_3$ at a mass ratio of 1:3:1 (α-cellulose: $(NH_4)_2C_2O_4{\cdot}H_2O$: $KHCO_3$) together and putting the mixture into a ceramic crucible. Then, the ceramic crucible was placed in a programmed temperature control furnace in a $N_2$ protection atmosphere where the mixture was calcined at 900 °C for 1 h and the heating rate was 10 °C/min. After being cooled down, the black powder was dissolved in 500 mL deionized water and magnetic stirred at room temperature for 24 h. Then, the solution was filtered and washed with deionized water until the pH of the filtrate reached 7. At last, the HPC-A was obtained after the black residue was dried at 105 °C in an oven overnight. For the preparation process of HPC-B, the difference from HPC-A is that the raw material is α-cellulose, $(NH_4)_2C_2O_4{\cdot}H_2O$, and $NaHCO_3$ at a mass ratio of 1:3:1 (α-cellulose: $(NH_4)_2C_2O_4{\cdot}H_2O$: $NaHCO_3$). And for the preparation process of HPC-C, the difference from HPC-A is that the raw material is α-cellulose and $K_2CO_3$ at a mass ratio of 1:3 (α-cellulose: $K_2CO_3$). Besides, a type of commercial activated carbon (AC) was obtained from a power plant.

### Adsorbents characterizations

The pore structure of adsorbents was determined by $N_2$ adsorption–desorption test at 77 K (Micromeritics ASAP 2460). Before each test, samples were degassed at 473 K for 12 h first. The specific surface area ($S_{BET}$) was estimated by the BET method. The micropore area and volume were calculated by t-plot method. The micropore distributions and the calculations

of ultramicropore (<0.7 nm) and micropres over 0.7 nm were analyzed by applying the nonlocal density functional theory (NLDFT) on the $N_2$ adsorption isotherms. The mesopore distributions were obtained from Barrett-Joyner-Halenda (BJH) method. The macropore distributions, density, and porosity of materials were measured by a mercury porosimeter (Auto Pore IV 9510). The microscopic morphology of adsorbents was observed by a scanning electron microscopy (SU-8010) at an accelerating voltage of 15.0 kV. The X-ray photoelectron spectra (XPS) of adsorbents were carried out by using the ESCALAB Mark II X-ray photoelectron spectroscopy in an ultra-high vacuum with aluminum magnesium binode (Al 1486.6 eV, Mg 1253.6 eV) X-ray source. The binding energy values were calibrated with respect to C1s peak (284.8 eV).

### *Toluene and $SO_2$ adsorption test*

The toluene and $SO_2$ dynamic adsorption tests were conducted on a self-build fixed bed dynamic adsorption system as shown in Fig S1. The high purity $N_2$ was used as the carrier gas, and the toluene steam was generated by the bubbling method; the toluene concentration can be controlled by adjusting the bubbling flow rate and the water bath temperature. $SO_2$ was generated by a gas cylinder of $SO_2$ calibration gas (2000 ppm), and the $SO_2$ concentration was controlled by adjusting the flow rate of the calibration gas. The fixed bed adsorption column is a quartz tube reactor with the internal diameter of 8 mm. The adsorption temperature was controlled by the thermostat of the temperature programmed vertical tube furnace, and the toluene and $SO_2$ adsorption was conducted at 303 K. The gas pressure of each adsorption test is atmospheric pressure and remains constant. The dosage of adsorbents was 50 mg for each adsorption test. In the single adsorption test, 500 ppm toluene or 500 ppm $SO_2$ gas was introduced into the adsorption column lonely. In the competitive adsorption test, 500 ppm toluene and 500 ppm $SO_2$ gas were mixed in the gas mixer first and then introduced into the adsorption column. The total flow rate of all the tests was 200 mL/min which was accurately controlled by the flowmeters (Beijing Sevenstar Electronics Co., Ltd.). The outlet toluene or $SO_2$ concentration was monitored online by a GASMET. The adsorption breakthrough curves of toluene or $SO_2$ can be obtained, and the adsorption capacity was calculated by following formula (Song et al. 2019; Meng et al. 2019):

$$q_t = \frac{Q\int_0^t (C_{in} - C_{out})dt}{m} \tag{1}$$

where $q_t$ (mg/g) is the adsorption capacity of toluene or $SO_2$ at time t, $C_{in}$ (mg/m$^3$) is the inlet concentration of toluene or $SO_2$, $C_t$ (mg/m$^3$) is the outlet concentration of toluene or $SO_2$ at time t, Q (mL/min) is the total gas flow rate, and m (g) is the dosage of the adsorbent. The adsorption capacity of materials is the $q_t$ when the dynamic adsorption reaches equilibrium.

### Toluene cyclic adsorption test

In order to reveal the adsorption reusability of adsorbent, a series of recycling tests were conducted on HPC-A. After the adsorption reached saturation, the desorption procedure was carried out under nitrogen gas flow at 300 °C until the toluene desorpted completely. And then toluene dynamic adsorption was tested again.

### Adsorption kinetics analysis

To analyze the adsorption kinetics of adsorbents, there are several classical models to fit the dynamic adsorption breakthrough curves, such as Yoon and Nelson (Y-N) model (Eq. (2)) (Kyung-Won et al. 2017; Ang et al. 2020), Thomas model (Eq. (3)) (Jafari et al. 2018; Cheng et al. 2020; Recepoğlu et al. 2018), and Adams-Bohart (A-B) model (Eq. (4)) (Kyung-Won et al. 2017; Khim Hoong 2020), expressed as follows.

$$t = \tau + \frac{1}{K_{YN}}\ln\frac{C}{C_0 - C} \tag{2}$$

$$\ln\left(\frac{C_0}{C} - 1\right) = K_T\left(\frac{q_0 m}{Q} - C_0 t\right) \tag{3}$$

$$\frac{C}{C_0} = \frac{e^{K_{AB}C_0 t}}{e^{(K_{AB}ZN_0)/U_0} - 1 + e^{K_{AB}C_0 t}} \tag{4}$$

where $t$(min) is the adsorption time, $C_0$ (mg/L) and $C$ (mg/L) are the inlet and outlet concentration, respectively, $K_{YN}$ (min$^{-1}$) is the Y-N rate constant, $q_0$ (mg/g) is the equilibrium adsorption capacity, $\tau$ (min) is the time required for 50% adsorption breakthrough, $m$ (g) is the dosage of adsorbent,$Q$ (mL/min) is the flow rate, $K_T$ (L·min$^{-1}$·mg$^{-1}$) is the Thomas rate constant, Z (cm) is the height of adsorbent column, $N_0$ (mg/L) is the volumetric adsorption capacity, $U_0$ (cm/min) is the flow linear velocity, and $K_{AB}$ (L·mg$^{-1}$·min$^{-1}$) is the Adams-Bohart rate constant.

For the fixed bed dynamic adsorption, generally believed it is a process that the mass transfer zone (MTZ) is established first, and then the MTZ moves in the adsorption column and finally moves out of the bed (Long. et al. 2012; Qian et al. 2019). In this process, the toluene molecules need to overcome various diffusion resistances to be adsorbed on the micropores of adsorbents. The length of mass transfer zone ($H_{MTZ}$) can be calculated by the following formulas (Eq. (5~6)).

$$f = \frac{\int_{T_{0.05}}^{T_{0.95}} (1 - C_0/C)dt}{T_{0.95} - T_{0.05}} \quad (5)$$

$$H_{MTZ} = \frac{(T_{0.95} - T_{0.05})Z}{\tau_e - (1-f)(T_{0.95} - T_{0.05})} \quad (6)$$

where $T_{0.05}$ (min) and $T_{0.95}$(min) are the time when the outlet concentration is 5% and 95% of the inlet concentration, respectively, $\tau_e$ (min) is the time when the adsorption reaches equilibrium, and $Z$ (mm) is the length of the adsorption bed.

## Results and discussion

### Characteristics of adsorbents

The $N_2$ adsorption–desorption isotherms of HPCs and AC are shown in Fig S2. Table 1 shows the pore specifications of materials derived from the $N_2$ adsorption–desorption isotherms and the density/porosity derived from the mercury porosimeter. It can be found that the HPC-A has the highest specific surface area and pore volume up to 2816 $m^2$/g and 1.413 $cm^3$/g as well as the highest microporosity of 83.51%. The HPC-B and HPC-C have similar specific surface area (~1400 $m^2$/g) and microporosity (~65%), while AC has the lowest specific surface area and pore volume. In observation of the ultramicropore (<0.7 nm) and the micropore of 0.7~2 nm, the HPC-A has the highest ratio of 0.7~2 nm micropore (pore volume 42.18%), while the HPC-C has the highest ratio of ultramicropore (pore volume 36.77%). It is worth noting that the HPC-C has the minimum average pore size (1.91 nm) though the microporosity of HPC-C is not the highest, and it can be attributed to the highest ratio of ultramicropore on HPC-C. Moreover, the HPC-A, HPC-B, and HPC-C are much lighter than the AC for they have similar lower density and higher porosity. For instance, the bulk densities of HPCs are in the range of 0.059~0.118 g/mL, but it is 0.543 g/mL for AC. The porosities of HPCs are all over 75%, and yet it is only 47.6% for the AC. The low density and high porosity can be attributed to the foaming action of the carbonates ($NaHCO_3$/$KHCO_3$/$K_2CO_3$) and $(NH_4)_2C_2O_4$ in the pore activation process of HPCs (Meng et al. 2019).

With regard to the pore size distributions of materials, Fig. 1 A and B show the micropore and mesopore distributions of adsorbents derived from $N_2$ adsorption–desorption isotherm and Fig. 1 C shows the macropore distributions of adsorbents derived from the mercury porosimetry. It can be observed that the HPC-A has the most abundant micropores of 0.7~2 nm and mesopores of 2~5 nm, but for the HPC-C and AC, the micropores over 0.7 nm and mesopores are fewer. The pore volume of HPC-A is the highest. It is worth noting that the HPC-B has more mesopores than HPC-C,

**Table 1** The pore specifications of adsorbents[a]

| Material | $S_{BET}$ ($m^2g^{-1}$) | Pore volume ($cm^3g^{-1}$) | Micro-porosity[b] | Average pore size (nm) | <0.7 nm[c] | | | 0.7~2 nm[c] | | | Bulk density (g/mL) | Apparent density (g/mL) | Porosity % |
|---|---|---|---|---|---|---|---|---|---|---|---|---|---|
| | | | | | Pore volume ($cm^3g^{-1}$) | Pore area ($m^2g^{-1}$) | Pore volume % | Pore volume ($cm^3g^{-1}$) | Pore area ($m^2g^{-1}$) | Pore volume % | | | |
| HPC-A (Lu et al. 2021) | 2816 | 1.413 | 83.51% | 2.01 | 0.120 | 487.26 | 8.49% | 0.596 | 1239.44 | 42.18% | 0.072 | 0.382 | 81.2 |
| HPC-B (Lu et al. 2021) | 1408 | 0.895 | 63.13% | 2.54 | 0.175 | 643.13 | 19.55% | 0.241 | 521.97 | 26.93% | 0.118 | 0.524 | 77.5 |
| HPC-C | 1320 | 0.631 | 66.77% | 1.91 | 0.232 | 821.20 | 36.77% | 0.206 | 374.18 | 32.65% | 0.059 | 0.354 | 83.3 |
| AC (Lu et al. 2021) | 688 | 0.406 | 62.87% | 2.36 | 0.101 | 372.36 | 24.88% | 0.112 | 235.07 | 27.59% | 0.543 | 1.036 | 47.6 |

[a]Derived from $N_2$ adsorption–desorption isotherm, and the density and porosity were derived from the mercury porosimeter

[b]The microporosity was obtained from t-plot calculation

[c]The pore area and volume of <0.7 nm and 0.7~2 nm were calculated by NLDFT method

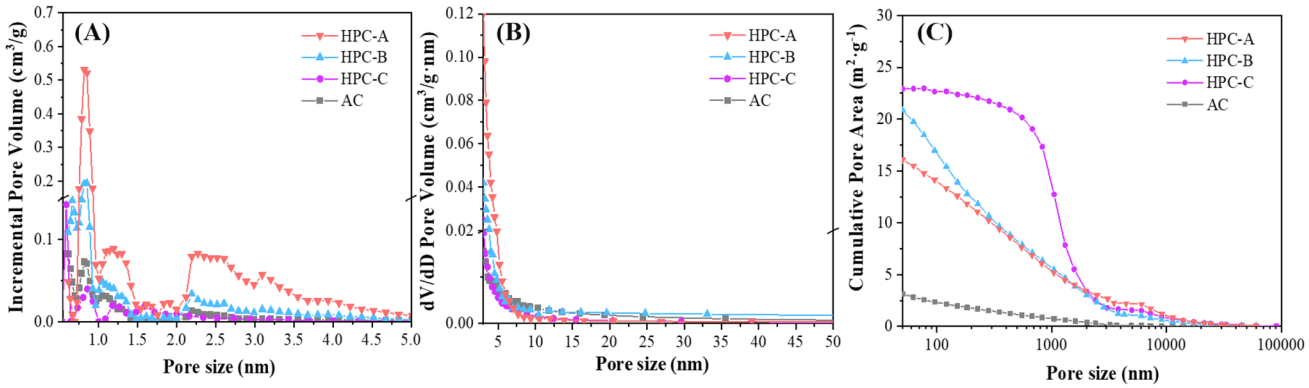


**Fig. 1** **A** Pore size distributions of 0.6 ~ 5 nm calculated by the NLDFT method; **B** pore size distributions of 3 ~ 50 nm calculated by the BJH method; **C** pore size distributions of macropores over 50 nm derived from the mercury porosimeter

and that lead to much higher pore volume of HPC-B (0.895 $cm^3/g$) than HPC-C (0.631 $cm^3/g$). There are much more macropores in HPCs compared with the AC, especially the macropores of the HPC-C are extremely substantial. It could be the reason why the HPC-C has the minimum density and maximum porosity over other three materials. The lack of mesopores and macropores leads to high density and low porosity of the AC. The results correspond to the pore specifications of materials in Table 1.

The morphologies of adsorbents were investigated by scanning electron microscopy (SEM) measurements. As Fig. 2 shows, the SEM images of HPC-A, HPC-B, and HPC-C show similar hierarchical porous structure with numerous meso-macropores ranging from tens of nanometers to several micrometers, especially the macropores of HPCs can be observed obviously. However, bulk morphology without apparent meso-macropores of AC can be seen in Fig. 2D (d). The hierarchical porous structure with abundant meso-macropores of HPCs results from the expanding gases (CO, $CO_2$, $NH_3$, etc.) from $KHCO_3$/$NaHCO_3$/$K_2CO_3$/$(NH_4)_2C_2O_4$ during the carbonization process (Tang et al. 2020). On closer inspection, the mesopores and micropores distributed on the carbon nanosheets can be observed especially on the HPC-A. However, nearly no mesopores can be found on the carbon nanosheets of the HPC-C, and it is probably because there are a large amount of ultramicropores that cannot be observed but much fewer micropores over 0.7 nm and mesopores on the HPC-C. The pore structure morphologies correspond to the pore size distributions of materials. To sum up, the HPCs are hierarchical porous carbon materials with large amount of mesopores or macropores. The HPC-A has abundant micropores over 0.7 nm but fewer ultramicropores, while the HPC-C has plenty of ultramicropores and macropores but lacks micropores over

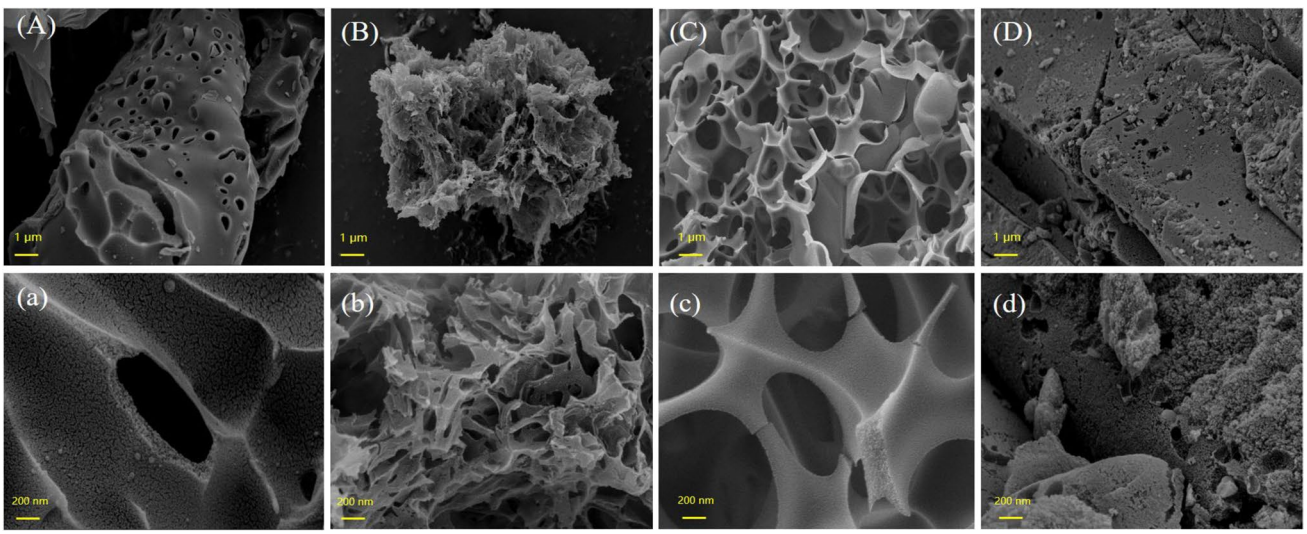


**Fig. 2** The SEM images of (**A**, a) HPC-A, (**B**, b) HPC-B, (**C**, c) HPC-C, (**D**, d) AC

0.7 nm. However, there are mainly micropores with very fewer mesopores and macropores on the AC.

Our previous work (Lu et al. 2021) and other related researches (Fan et al. 2013; Xi et al. 2019; Yang et al. 2020) which used $K_2CO_3$/$KHCO_3$/$NaHCO_3$ as activator to activate carbon materials revealed that the pore formation mechanism of HPCs can be described as Fig S3 shows. Besides, our previous work (Lu et al. 2021) also emphasized the activation of $(NH_4)_2C_2O_4$, and revealed that the hierarchical porous structure of HPCs can be attributed to the foaming action by $CO_2$ or $NH_3$ molecules which come from the decomposition of $(NH_4)_2C_2O_4$, $NaHCO_3$/$KHCO_3$, or $K_2CO_3$. As the reactivity of $KHCO_3$ is higher than $NaHCO_3$ (Lu et al. 2021), the HPC-A has more abundant micropores and mesopores but fewer macropores than HPC-B.

The X-ray photoelectron spectroscopy analysis was conducted to characterize the chemical composition, especially the nitrogen content doped in HPC-A and HPC-B; the XPS wide scan spectrum can be seen in Fig S4, and the deconvolutions of the XPS curves (N1s) of HPC-A and HPC-B can be found in our previous work (Lu et al. 2021). The semi-quantitative data derived from XPS measurements (Table S1) showed that the N-Atomic % of HPC-A and HPC-B is 2.03% and 1.59%, respectively. The nitrogen content in HPC-A and HPC-B can be attributed to the activation of $(NH_4)_2C_2O_4$ (Tang et al. 2020).

### *Toluene and $SO_2$ adsorption capacity*

The toluene and $SO_2$ dynamic adsorption tests were conducted to calculate the equilibrium adsorption capacity, and the results are shown in Table 2. It can be obviously found that the adsorption capacity of toluene for all the materials is much higher than that of $SO_2$, especially the HPC-A. Related researches about co-adsorption of toluene and $SO_2$ also revealed similar phenomenon (Qie et al. 2019, 2020). Noticeably, the toluene single adsorption capacity of HPC-A is particularly high (585 mg/g), it is about 3 times higher than that of the AC (205 mg/g), and it is higher than many other carbon adsorbents in related researches (Zhang et al. 2017). The high toluene adsorption capacity of HPC-A can be attributed to its high micropore area and volume (Lu et al. 2021). However, the $SO_2$ single adsorption capacity of HPC-A is relatively lower than HPC-B and HPC-C. Significantly, the $SO_2$ single adsorption capacity of HPC-C is particularly higher than other three adsorbents even though the microporosity of HPC-C is not the highest. This is probably due to the richer ultramicropore on HPC-C in contrast with other adsorbents as related research (Raymundo-Piñero et al. 2000) reported the $SO_2$ adsorption capacity tend to be associated with the ultramicropore of adsorbents. Besides, some researches about $SO_2$ adsorption by nitrogen-doped carbon materials revealed that the nitrogenous functional groups in carbon adsorbents have a definite promotional effect for $SO_2$ adsorption (Zhang et al. 2020; Sun et al. 2016b). Jingai Shao et al. (2018) even revealed that the nitrogen functional groups on the surface of the nitrogen-enriched biochar are more effective than the pore structure for $SO_2$ adsorption. Though the HPC-A (2.03% N-Atomic) and HPC-B (1.59% N-Atomic) have nitrogen doping, even the HPC-A has more developed pore structure and much higher microporosity, the $SO_2$ single adsorption capacity of HPC-A is much lower than HPC-C. Thus, there must be more significant factors that dominate the toluene and $SO_2$ adsorption capacity.

The correlation analyses between toluene and $SO_2$ single adsorption capacity and pore structure parameters (pore volume and area of < 0.7 nm and 0.7 ~ 2 nm) derived from $N_2$ adsorption–desorption tests were conducted as Fig. 3A ~ D shows. There are high correlations between the $SO_2$ adsorption capacity and the pore volume of < 0.7 nm ($R^2 = 0.9765$) and pore area of < 0.7 nm ($R^2 = 0.9452$) (Fig. 3A, B). As the dynamics diameter of $SO_2$ molecular is 0.28 nm (Qie et al. 2019), it can be inferred that the ultramicropores dominate the $SO_2$ dynamic adsorption capacity of adsorbents in this work. And E. Raymundo-Pinero et al. (2000) had revealed that the $SO_2$ adsorption capacity tend to increase as the ultramicropore volume of adsorbents increased. The dynamic diameter of $CO_2$ (0.33 nm) (Zubbri et al. 2020) is close to that of $SO_2$ (0.28 nm). Chang et al. (2019) synthetized N-doped hierarchical porous carbon derived from

**Table 2** The toluene and $SO_2$ adsorption capacity of materials

| Material | Toluene adsorption capacity (mg/g) | | Difference | $SO_2$ adsorption capacity (mg/g) | | Difference | T/S* |
|---|---|---|---|---|---|---|---|
| | Single[d] | Competitive[e] | | Single[d] | Competitive[e] | | |
| HPC-A | 585 (Lu et al. 2021) | 562 | −3.93% | 14.3 | 11.0 | −23.00% | 40.91 |
| HPC-B | 342 (Lu et al. 2021) | 328 | −4.09% | 18.0 | 15.6 | −12.89% | 19.00 |
| HPC-C | 336 | 315 | −6.85% | 24.4 | 23.7 | −2.87% | 13.77 |
| AC | 205 (Lu et al. 2021) | 185 | −9.76% | 12.9 | 12.4 | −3.96% | 15.89 |

[d]Single toluene/$SO_2$ adsorption test

[e]Competitive adsorption test

*Toluene single adsorption capacity/$SO_2$ single adsorption capacity

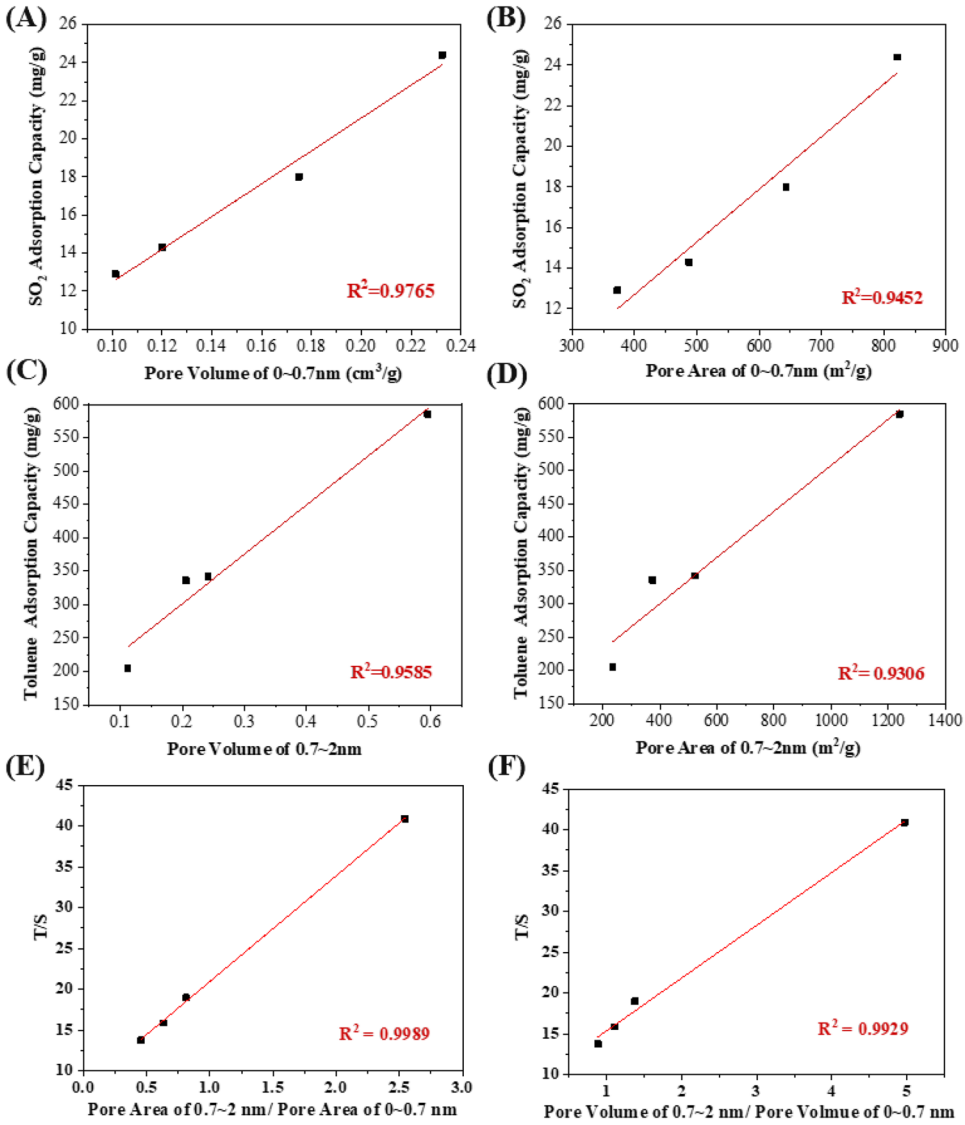


**Fig. 3** The relationship between $SO_2$ adsorption capacities and **A** pore volume of < 0.7 nm; **B** pore area of < 0.7 nm. The relationship between Toluene adsorption capacities and **C** pore volume of 0.7 ~ 2 nm; **D** pore area of 0.7 ~ 2 nm. The correlation between T/S and **E** pore area of 0.7 ~ 2 nm/ pore area of < 0.7 nm, **F** pore volume of 0.7 ~ 2 nm/pore volume < 0.7 nm

poplar catkin to adsorb $CO_2$ and found that the micropores of < 1 nm in size as well as nitrogen species lead to remarkable $CO_2$ adsorption performance. Shi et al. (2021) studied $CO_2$ adsorption by microporous carbon nanosheets and revealed that the high uptake, moderate adsorption heat, good selectivity, and superior recyclability for $CO_2$ capture can be attributed to the large surface area, high density of narrow micropores, and adjustable and large-proportioned ultramicroporosity. It can be inferred that for small molecule adsorbates ($CO_2$, $SO_2$, etc.) dynamic adsorption, the ultramicropore of adsorbents determines the adsorption properties.

For the toluene adsorption, as Fig. 3 C and D show, there are high correlations between the toluene adsorption capacity and the pore volume of 0.7 ~ 2 nm ($R^2 = 0.9585$) and pore area of 0.7 ~ 2 nm ($R^2 = 0.9306$). As the dynamics diameter of toluene molecular is 0.68 nm (Qie et al. 2019), it can be inferred that the micropores over 0.7 nm dominate the toluene adsorption capacity of adsorbents. There are deeper discussions in this work as related researches (Lillo-Ródenas et al. 2005; Jin et al. 2020) and our previous work (Lu et al. 2021) found that the toluene adsorption capacity is mainly determined by the micropores of adsorbents rather than the mesopores and macropores. Furthermore, as Fig S5 shows, there is no relevance between the toluene adsorption capacity and pore area or pore volume of < 0.7 nm and so does the relationship between $SO_2$ adsorption capacity and pore area or pore volume of 0.7 ~ 2 nm.

Though both the toluene and $SO_2$ are mainly adsorbed on the microporous surface as many researches had reported, the micropore distributions of adsorbents dominate the adsorption capacity of toluene and $SO_2$. The T/S (toluene single adsorption capacity/$SO_2$ single adsorption capacity) of adsorbents is HPC-A > HPC-B > AC > HPC-C as Table 2 shows. It

reveals that the HPC-A has more toluene adsorption sites compared with $SO_2$, the HPC-B followed, and then the AC, yet the adsorption sites of $SO_2$ on HPC-C are the most abundant relatively. A higher T/S means a higher adsorption selectivity of toluene compared with $SO_2$. As Fig. 3 E and F show, the T/S has high correlations with the pore are of 0.7 ~ 2 nm/pore area of < 0.7 nm ($R^2 = 0.9989$) and pore volume of 0.7 ~ 2 nm/pore volume of < 0.7 nm ($R^2 = 0.9929$). Thus, the micropore distribution of ultramicropore and micropores over 0.7 nm can interpret why the HPC-A has the highest toluene adsorption capacity but a lower $SO_2$ adsorption capacity, while the HPC-C has the highest $SO_2$ adsorption capacity but a lower toluene adsorption capacity.

For the competitive adsorption of toluene and $SO_2$, as Table 2 shows, a higher T/S leads to a lower toluene adsorption reduction but higher $SO_2$ adsorption capacity decrease. For instance, the toluene adsorption capacity reduction of HPC-A is the lowest (− 3.93%), while for the $SO_2$, it is the highest (− 23.00%). However, for HPC-C, the $SO_2$ adsorption capacity reduction is the lowest (− 2.87%), but the toluene adsorption capacity decrease is relatively high (− 6.85%). The T/S is determined by the micropore distribution of adsorbents (Fig. 3E, F). It can be concluded that the micropore distribution dominates the adsorption capacity and selectivity of toluene and $SO_2$. The ultramicropore are conducive to the $SO_2$ adsorption, and the micropores over 0.7 nm are beneficial for the toluene adsorption.

### *Toluene and $SO_2$ adsorption kinetics*

For all the dynamic adsorption tests, the dosage of the adsorbents was 50 mg. The length of the adsorption bed for HPC-A, HPC-B, HPC-C, and AC were 6 mm, 6 mm, 8 mm, and 3 mm, respectively, due to the great bulk density differences of HPCs and AC.

The dynamic adsorption breakthrough curve measurement is an effective way to make clear the adsorption kinetics of adsorbents, and the toluene breakthrough curves of single and competitive adsorption are as shown in Fig. 4A ~ D. The adsorption breakthrough and saturation time as well as the calculation of $H_{MTZ}$ of adsorbents are shown in Table S2. Generally, in the case of the same adsorption condition, a longer breakthrough time means a higher dynamic adsorption capacity, and a more rapid increase of the breakthrough curve indicates a higher adsorption diffusion rate. The HPC-A has the longest breakthrough time (82 min) with a rapid increase of the breakthrough curves, while the AC has the shortest breakthrough time (13 min) and the breakthrough curve increases slowly. It can be inferred that the HPC-A has excellent toluene adsorption properties with high adsorption capacity and great adsorption kinetics, yet the AC is not a good adsorbents for toluene adsorption. Meanwhile, comparing the single toluene adsorption and competitive adsorption, the toluene breakthrough curves of HPC-B and HPC-C become steeper, while the shape of the toluene breakthrough curve of HPC-A hardly changed, but for AC, it becomes smoother. It can be deduced that the $SO_2$ has certain influences on the toluene adsorption kinetics.

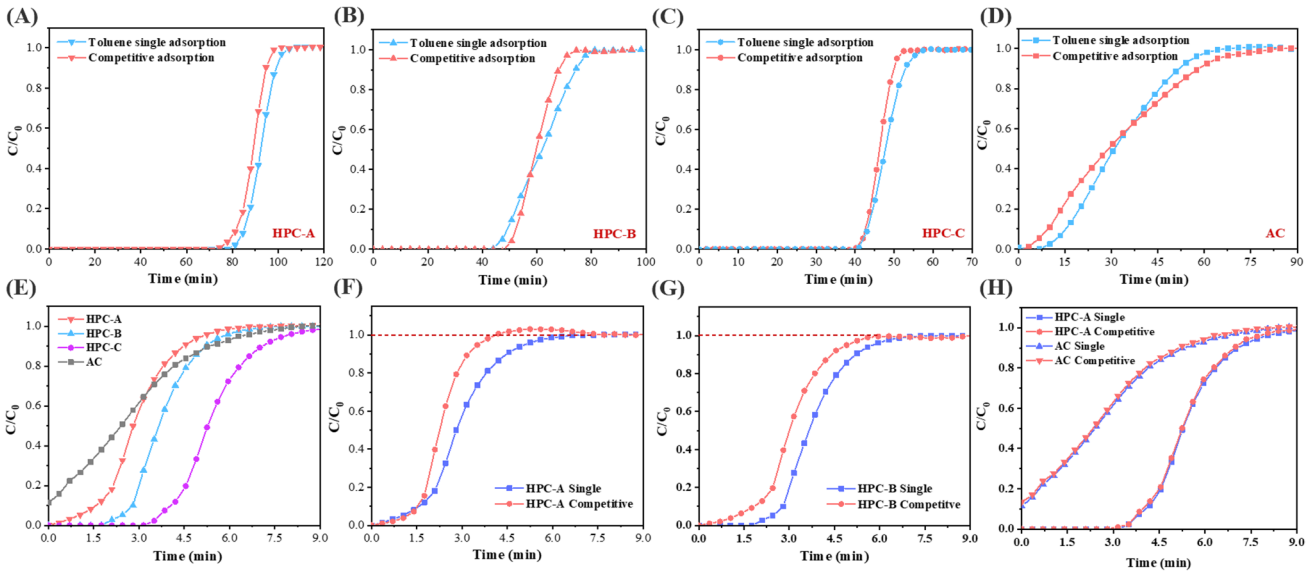


**Fig. 4** The single toluene and competitive adsorption toluene breakthrough curves of **A** HPC-A; **B** HPC-B; **C** HPC-C; **D** AC. **E** The single $SO_2$ adsorption breakthrough curves of materials. The $SO_2$ breakthrough curves of single adsorption and competitive adsorption of **F** HPC-A; **G** HPC-B; **H** HPC-C and AC

The fitting results of the toluene dynamic adsorption breakthrough curves through Y-N, Thomas, and A-B models and the calculation of $H_{MTZ}$ are shown in Table 3. The fitting curves of the three models present very high correlation coefficients ($R^2 > 0.99$) for all the adsorbents. For the single toluene adsorption, the $H_{MTZ}$ (HPC-A) < $H_{MTZ}$ (HPC-C) < $H_{MTZ}$ (HPC-B) < $H_{MTZ}$ (AC), it demonstrates that the toluene molecules diffusion resistance of HPC-A is the least, but for the AC, it is the maximal. Besides, the $K_{YN}$, $K_T$, and $K_{AB}$ of HPCs are much higher than the AC, which reveals that HPCs have much higher toluene adsorption rate and lower toluene molecules diffusion resistance. Chao Long et al. (2012) had revealed that the meso-macropores of adsorbents can act as the transport channels for VOCs molecules diffusing into the micropore and internal surfaces, and our previous work (Tang et al. 2020) also reached this conclusion. Therefore, the great toluene adsorption kinetics of HPCs can be attributed to the hierarchical porous structures with abundant meso-macropores.

The τ, $q_0$, and $N_0$ for competitive adsorption decreased together with the toluene adsorption capacity compared with the single toluene adsorption. Comparing the toluene adsorption kinetics of single toluene adsorption and competitive adsorption, the variations of $K_{YN}$, $K_T$, $K_{AB}$, and $H_{MTZ}$ are shown in Fig S6. It can be found that the $K_{YN}$, $K_T$, $K_{AB}$, and $H_{MTZ}$ of HPC-A have little change. Meanwhile, for the HPC-B and HPC-C, the $H_{MTZ}$ decreased, while the $K_{YN}$, $K_T$, and $K_{AB}$ increased, but for the AC, the tendency is in contrary. Thus, for the HPC-A, the $SO_2$ has little effect on toluene adsorption kinetics; for the HPC-B and HPC-C, the $SO_2$ promotes the toluene adsorption kinetics. However, for the AC, the $SO_2$ is not conducive to the toluene adsorption kinetics. It can be inferred that the $SO_2$ promotes the diffusion of toluene molecules on HPC-B and HPC-C, while it hinders the toluene diffusion on AC. The pore size distributions of adsorbents could have significant impacts on this phenomenon.

With regard to the $SO_2$ adsorption, the $SO_2$ breakthrough curves of adsorbents are shown in Fig. 4E ~ H. It can be found that the breakthrough curves of HPCs are relatively steeper than the AC as Fig. 4E shows. Thus, less $SO_2$ molecules diffusion resistance on HPCs can be inferred, and that can be attributed to the hierarchical porous structure of HPCs. Comparing the $SO_2$ breakthrough curves between single and competitive adsorption, it is remarkable that a $SO_2$ desorption phenomenon can be found on HPC-A when competitive adsorption as Fig. 4F shows, while the breakthrough time of the competitive adsorption is advanced on HPC-B as Fig. 4G shows. However, the $SO_2$ breakthrough curves of HPC-C and AC have hardly changed between single and competitive adsorption as Fig. 4H shows. It can be inferred that the $SO_2$ molecules are very easy to desorb and even replaced by toluene molecules on HPC-A due to its abundant micropores over 0.7 nm and rich mesopores. The $SO_2$ adsorption is basically unaffected by toluene on HPC-C and AC due to their rare mesopores and fewer micropores over 0.7 nm.

It can be concluded that the pore size distributions of adsorbents dominate the adsorption selectivity and kinetics of toluene and $SO_2$. The adsorption mechanism can be described as Fig. 5 shows. For the dynamic adsorption on carbon adsorbents, the $SO_2$ molecules are mainly adsorbed on ultramicropore, and the toluene molecules are mainly adsorbed on the surface of the micropores over 0.7 nm. Mesopores and macropores can decrease the adsorption diffusion resistance of toluene and $SO_2$ molecules. Qie et al. (2019) used the MD simulation to analyze $SO_2$ and toluene combined adsorption on hierarchical pore models and revealed that the micropore is mostly occupied by $SO_2$ molecules, while toluene molecules tend to store in large-sized micropores or mesopores. As the micropores which increase the toluene adsorption diffusion resistance had occupied by $SO_2$ molecules, the adsorption diffusion resistance of toluene molecules decreased relatively, and the toluene adsorption

**Table 3** The fitting parameters of toluene adsorption breakthrough curves and calculation of $H_{MTZ}$

| Material | | Y-N model | | Thomas model | | Adams-Bohart model | | $R^2$ | $H_{MTZ}$ |
|---|---|---|---|---|---|---|---|---|---|
| | | $K_{YN}$ | τ | $K_T$ | $q_0$ | $K_{AB}$ | $N_0$ | | |
| HPC-A | Single[f] | 0.32 | 92.37 | 0.19 | 624.42 | 0.19 | $1.04\times10^5$ | 0.9998 | 1.24 |
| | Competitive[g] | 0.35 | 88.98 | 0.21 | 597.93 | 0.21 | $9.97\times10^4$ | 0.9996 | 1.28 |
| HPC-B | Single[f] | 0.17 | 61.65 | 0.12 | 350.18 | 0.12 | $5.84\times10^4$ | 0.9980 | 3.01 |
| | Competitive[g] | 0.28 | 59.89 | 0.20 | 330.57 | 0.20 | $5.51\times10^4$ | 0.9990 | 2.10 |
| HPC-C | Single[f] | 0.46 | 47.78 | 0.26 | 342.1 | 0.26 | $4.28\times10^4$ | 0.9996 | 2.17 |
| | Competitive[g] | 0.62 | 46.24 | 0.35 | 331.08 | 0.35 | $4.14\times10^4$ | 0.9998 | 1.73 |
| AC | Single[f] | 0.12 | 32.01 | 0.07 | 208.69 | 0.07 | $1.05\times10^4$ | 0.9980 | 3.68 |
| | Competitive[g] | 0.08 | 30.68 | 0.06 | 186.54 | 0.06 | $9.59\times10^4$ | 0.9990 | 5.03 |

[f]Single toluene adsorption test

[g]Competitive adsorption test

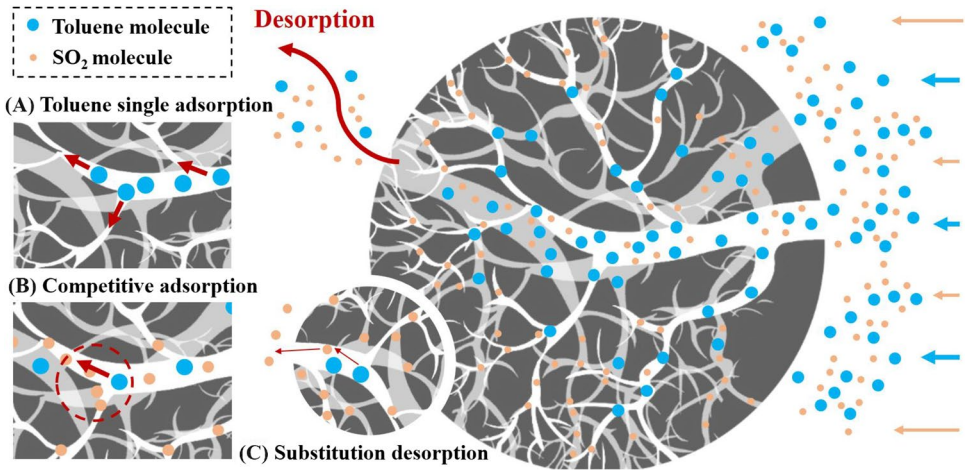


**Fig. 5** The simulation diagram of toluene and $SO_2$ adsorption mechanism

kinetics improved on HPC-B and HPC-C when competitive adsorption as a result. For the micropores over 0.7 nm and mesopores, the toluene molecules are more easily adsorbed, while the $SO_2$ molecules can be easily desorbed or even replaced by toluene molecules as Fig. 5C shows. Thus, the $SO_2$ desorption phenomenon on HPC-A when competitive adsorption can be attributed to the rich micropores over 0.7 nm and mesopores.

## Toluene cyclic adsorption

As mentioned above, the HPC-A has the best toluene adsorption performance with the highest toluene adsorption capacity and selectivity. In practical application of carbon adsorbents, it is necessary to consider the desorption characteristics which is greatly dependent on the pore network developed in the adsorbent and the surface properties of adsorbents (Seung Won et al. 2012). To reveal the reusability (stability and reproducibility) of adsorbents, the toluene cyclic adsorption tests were conducted on the HPC-A. As shown in Fig. 6 and Table S3, after 4 cyclic adsorption–desorption tests, the adsorption capacity of toluene maintained at 90% (538 mg/g). There is a larger reduction (5%) of toluene adsorption capacity at the first cyclic adsorption. But only 2% reduction of the capacity was found on the next 2 ~ 4 cyclic adsorption. Baytar et al. (2020) did the benzene and toluene cyclic adsorption–desorption test to determine the reusability performance of AC, found that the benzene and toluene adsorption capacity decreased slightly by 8.10% and 7.42% after five cycles, and revealed that it was due to the deformation of the adsorbent when it was used again or due to the saturation of the adsorbent surface. It can be inferred that the HPC-A has good reusability properties in practical application, and it can be an appropriative adsorbent with great application potential for VOCs adsorption in coal-fired flue gas.

## Conclusions

Various hierarchical porous carbons (HPCs) with different pore size distributions were synthesized in this work. The toluene, $SO_2$ single, and competitive dynamic adsorption tests were conducted on HPCs and a type of commercial activated carbon (AC). The mechanism of toluene and $SO_2$, adsorption capacity, selectivity, and kinetics were revealed in

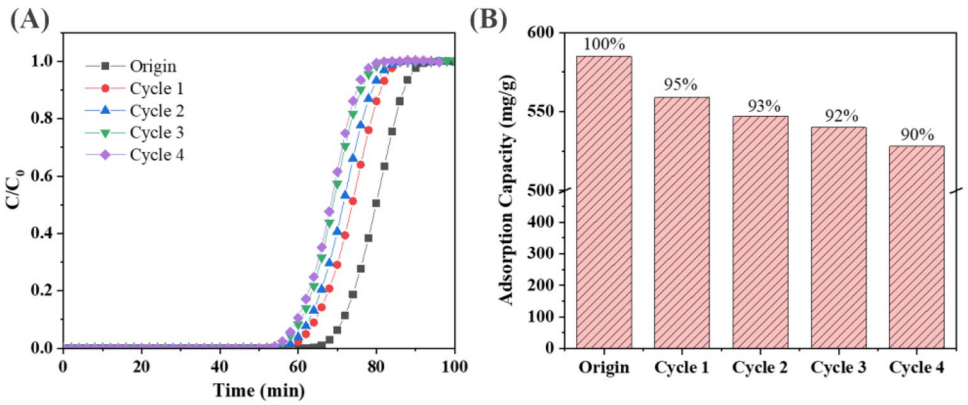


**Fig. 6** **A** The toluene cyclic adsorption breakthrough curves of HPC-A; **B** the toluene cyclic adsorption capacity change of HPC-A

this work. The $SO_2$ molecules are mainly adsorbed on ultramicropore, and the toluene molecules are mainly adsorbed on the surface of the micropores over 0.7 nm. The ultramicropores determine the $SO_2$ adsorption capacity and promote the $SO_2$ adsorption selectivity, while the micropores of 0.7 ~ 2 nm and mesopores are beneficial for toluene adsorption. The pore size distributions of adsorbents dominate the adsorption selectivity of toluene and $SO_2$, a higher ratio of ultramicropore shows higher $SO_2$ adsorption capacity and selectivity, and a higher proportion of micropores over 0.7 nm shows higher toluene adsorption capacity and selectivity. The $SO_2$ can promote the toluene adsorption kinetics on hierarchical porous carbons, which can be interpreted as the $SO_2$ molecules reduce the adsorption diffusion resistance of toluene molecules through occupying ultramicropores when competitive adsorption. The HPC-A proposed in this work has high toluene adsorption selectivity, capacity (585 mg/g), and excellent toluene adsorption kinetics. The toluene cyclic adsorption tests of HPC-A showed that, after 4 cyclic adsorption–desorption tests, the adsorption capacity of toluene maintained at 90% (528 mg/g). The HPC-A can be an appropriative adsorbent with great application potential for VOCs adsorption in coal-fired flue gas.

**Supplementary Information** The online version contains supplementary material available at https://doi.org/10.1007/s11356-021-18380-8.

**Author contribution** Xinlei Huang: Experimental design, date analysis, and writing the original draft manuscript. Hongxian Li and Ling Wang: Experimental and analysis. Minghui Tang: Conceptualization, investigation, methodology, review and editing, and funding. Shengyong Lu: Supervision, investigation, and conceptualization. All authors agree to be accountable for all aspects of the work in ensuring that questions related to the accuracy or integrity of any part of the work are appropriately investigated and resolved.

**Funding** This work was financially supported by the National Natural Science Foundation of China (No. 52006191), the Natural Science Foundation of Zhejiang Province (No. LY21E060007), the Fundamental Research Funds for the Central Universities (No. 2021QNA4005), and the Independent project of State key Laboratory (ZJUCEU2021010).

**Data availability** All data and materials generated or analyzed during this study were included in this published article and its supplementary information files.

## Declarations

**Ethics approval** The paper is a conceptualization and analysis of the published literature on the topic. No human subjects or animals were used in this paper.

**Consent to participate** Not applicable.

**Consent for publication** Not applicable.

**Competing interests** The authors declare no competing interests.

## References

Ang TN, Young BR, Taylor M, Burrell R, Aroua MK, Baroutian S (2020) Breakthrough analysis of continuous fixed-bed adsorption of sevoflurane using activated carbons. Chemosphere 239:124839. https://doi.org/10.1016/j.chemosphere.2019.124839

Baytar O, Şahin Ö, Horoz S, Kutluay S (2020) High-performance gas-phase adsorption of benzene and toluene on activated carbon: response surface optimization, reusability, equilibrium, kinetic, and competitive adsorption studies. Environ Sci Pollut Res 27(21):26191–26210. https://doi.org/10.1007/s11356-020-08848-4

Chang B, Shi W, Yin H, Zhang S, Yang B (2019) Poplar catkin-derived self-templated synthesis of N-doped hierarchical porous carbon microtubes for effective CO2 capture. Chem Eng J 358:1507–1518. https://doi.org/10.1016/j.cej.2018.10.142

Cheng H, Sun Y, Wang X, Zou S, Ye G, Huang H, Ye D (2020) Hierarchical porous carbon fabricated from cellulose-degrading fungus modified rice husks: ultrahigh surface area and impressive improvement in toluene adsorption. J Hazard Mater 392:122298. https://doi.org/10.1016/j.jhazmat.2020.122298

Cheng T, Li J, Ma X, Zhou L, Wu H, Yang L (2021) The adsorption properties of microporous activated carbon prepared from pistachio nut shell for low-concentration VOCs under low-medium temperatures. Environ Sci Pollut Res. https://doi.org/10.1007/s11356-021-14586-y

Deng L, Lu B, Li J, Lv G, Du S, Shi J, Yang Y (2017) Effect of pore structure and oxygen-containing groups on adsorption of dibenzothiophene over activated carbon. Fuel 200:54–61. https://doi.org/10.1016/j.fuel.2017.03.018

Fan X, Zhang L, Zhang G, Shu Z, Shi J (2013) Chitosan derived nitrogen-doped microporous carbons for high performance CO2 capture. Carbon 61:423–430. https://doi.org/10.1016/j.carbon.2013.05.026

Gil RR, Ruiz B, Lozano MS, Martín MJ, Fuente E (2014) VOCs removal by adsorption onto activated carbons from biocollagenic wastes of vegetable tanning. Chem Eng J 245:80–88. https://doi.org/10.1016/j.cej.2014.02.012

He G, He H (2016) DFT studies on the heterogeneous oxidation of SO(2) by oxygen functional groups on graphene. Phys Chem Chem Phys 18(46):31691–31697. https://doi.org/10.1039/c6cp06665h

Jafari S, Ghorbani-Shahna F, Bahrami A, Kazemian H (2018) Adsorptive removal of toluene and carbon tetrachloride from gas phase using zeolitic imidazolate framework-8: effects of synthesis method, particle size, and pretreatment of the adsorbent. Microporous Mesoporous Mater 268:58–68. https://doi.org/10.1016/j.micromeso.2018.04.013

Jin Z, Wang B, Ma L, Fu P, Xie L, Jiang X, Jiang W (2020) Air preoxidation induced high yield N-doped porous biochar for improving toluene adsorption. *Chem Eng J 385*. https://doi.org/10.1016/j.cej.2019.123843

Khim Hoong C (2020) Breakthrough curve analysis by simplistic models of fixed bed adsorption: in defense of the century-old Bohart-Adams model. Chem Eng J 380:122513. https://doi.org/10.1016/j.cej.2019.122513

Kim K-J, Ahn H-G (2012) The effect of pore structure of zeolite on the adsorption of VOCs and their desorption properties by microwave heating. Microporous Mesoporous Mater 152:78–83. https://doi.org/10.1016/j.micromeso.2011.11.051

Kyung-Won J, Tae-Un J, Jae-Woo C, Kyu-Hong A, Sang-Hyup L (2017) Adsorption of phosphate from aqueous solution using electrochemically modified biochar calcium-alginate beads: batch and fixed-bed column performance. Bioresour Technol 244(Pt 1):23–32. https://doi.org/10.1016/j.biortech.2017.07.133

Li L, Liu S, Liu J (2011) Surface modification of coconut shell based activated carbon for the improvement of hydrophobic VOC removal. J Hazard Mater 192(2):683–690. https://doi.org/10.1016/j.jhazmat.2011.05.069

Li X, Ma J, Ling X (2020) Design and dynamic behaviour investigation of a novel VOC recovery system based on a deep condensation process. Cryogenics 107:103060. https://doi.org/10.1016/j.cryogenics.2020.103060

Lillo-Ródenas MA, Cazorla-Amorós D, Linares-Solano A (2005) Behaviour of activated carbons with different pore size distributions and surface oxygen groups for benzene and toluene adsorption at low concentrations. Carbon 43(8):1758–1767. https://doi.org/10.1016/j.carbon.2005.02.023

Lim J, Cho H, Kim J (2021) Optimization of wet flue gas desulfurization system using recycled waste oyster shell as high-grade limestone substitutes. J Clean Prod 318:128492. https://doi.org/10.1016/j.jclepro.2021.128492

Long C, Li Y, Yu W, Li A (2012) Removal of benzene and methyl ethyl ketone vapor: comparison of hypercrosslinked polymeric adsorbent with activated carbon. J Hazard Mater 203–204:251–256. https://doi.org/10.1016/j.jhazmat.2011.12.010

Lu S, Huang X, Tang M, Peng Y, Wang S, Makwarimba CP (2021) Synthesis of N-doped hierarchical porous carbon with excellent toluene adsorption properties and its activation mechanism. Environ Pollut 284:117113. https://doi.org/10.1016/j.envpol.2021.117113

Ma X, Lv H, Yang L, Zhang Z, Sun Z, Wu H (2021) Removal characteristics of organic pollutants by the adsorbent injection coupled with bag filtering system. J Hazard Mater 405:124193. https://doi.org/10.1016/j.jhazmat.2020.124193

Meng F, Song M, Wei Y, Wang Y (2019) The contribution of oxygen-containing functional groups to the gas-phase adsorption of volatile organic compounds with different polarities onto lignin-derived activated carbon fibers. Environ Sci Pollut Res Int 26(7):7195–7204. https://doi.org/10.1007/s11356-019-04190-6

Mohan N, Kannan GK, Upendra S, Subha R, Kumar NS (2009) Breakthrough of toluene vapours in granular activated carbon filled packed bed reactor. J Hazard Mater 168(2–3):777–781. https://doi.org/10.1016/j.jhazmat.2009.02.079

Muñoz R, Souza TSO, Glittmann L, Pérez R, Quijano G (2013) Biological anoxic treatment of O2-free VOC emissions from the petrochemical industry: a proof of concept study. J Hazard Mater 260:442–450. https://doi.org/10.1016/j.jhazmat.2013.05.051

Padhi SK, Gokhale S (2014) Biological oxidation of gaseous VOCs-rotating biological contactor a promising and eco-friendly technique. J Environ Chem Eng 2(4):2085–2102. https://doi.org/10.1016/j.jece.2014.09.005

Qian W, Song Q, Ding H, Xie W (2019) Computational simulations of the mass transfer zone in GS adsorption column packed with Fe(3+) type ion exchanger. Chemosphere 215:507–514. https://doi.org/10.1016/j.chemosphere.2018.10.054

Qie Z, Sun F, Zhang Z, Pi X, Qu Z, Gao J, Zhao G (2020) A facile trace potassium assisted catalytic activation strategy regulating pore topology of activated coke for combined removal of toluene/SO2/NO. Chem Eng J 389:124262. https://doi.org/10.1016/j.cej.2020.124262

Qie Z, Zhang Z, Sun F, Wang L, Pi X, Gao J, Zhao G (2019) Effect of pore hierarchy and pore size on the combined adsorption of SO2 and toluene in activated coke. Fuel 257:116090. https://doi.org/10.1016/j.fuel.2019.116090

Raymundo-Piñero E, Cazorla-Amorós D, Salinas-Martinez de Lecea C, Linares-Solano A (2000) Factors controling the SO2 removal by porous carbons: relevance of the SO2 oxidation step. Carbon 38(3):335–344. https://doi.org/10.1016/S0008-6223(99)00109-8

Recepoğlu YK, Kabay N, Ipek IY, Arda M, Yüksel M, Yoshizuka K, Nishihama S (2018) Packed bed column dynamic study for boron removal from geothermal brine by a chelating fiber and breakthrough curve analysis by using mathematical models. Desalination 437:1–6. https://doi.org/10.1016/j.desal.2018.02.022

Rodrigues IN, de Medeiros JL, Araújo OdQF (2021) Sulfite removal from flue-gas desulfurization residues of coal-fired power plants: oxidation experiments and kinetic parameters estimation. Energy Rep. https://doi.org/10.1016/j.egyr.2021.04.062

Seung Won N, Wang Geun S, Young-Kwon P, Sang Chai K (2012) Thermal and chemical regeneration of spent activated carbon and its adsorption property for toluene. Chem Eng J 210:500–509. https://doi.org/10.1016/j.cej.2012.09.023

Shao J, Zhang J, Zhang X, Feng Y, Zhang H, Zhang S, Chen H (2018) Enhance SO2 adsorption performance of biochar modified by CO2 activation and amine impregnation. Fuel 224:138–146. https://doi.org/10.1016/j.fuel.2018.03.064

Shi W, Zhang Q, Liu S, Su S, Chang B, Yang B (2021) Copper ions-assisted inorganic dynamic porogen of graphene-like multiscale microporous carbon nanosheets for effective carbon dioxide capture. J Colloid Interface Sci 600:670–680. https://doi.org/10.1016/j.jcis.2021.04.146

Song M, Yu L, Song B, Meng F, Tang X (2019) Alkali promoted the adsorption of toluene by adjusting the surface properties of lignin-derived carbon fibers. Environ Sci Pollut Res Int 26(22):22284–22294. https://doi.org/10.1007/s11356-019-05456-9

Sun F, Gao J, Liu X, Yang Y, Wu S (2016a) Controllable nitrogen introduction into porous carbon with porosity retaining for investigating nitrogen doping effect on SO2 adsorption. Chem Eng J 290:116–124. https://doi.org/10.1016/j.cej.2015.12.044

Sun F, Gao J, Liu X, Yang Y, Wu S (2016b) Controllable nitrogen introduction into porous carbon with porosity retaining for investigating nitrogen doping effect on SO 2 adsorption. Chem Eng J 290:116–124. https://doi.org/10.1016/j.cej.2015.12.044

Tang L, Qu J, Mi Z, Bo X, Chang X, Anadon LD, Wang S, Xue X, Li S, Wang X, Zhao X (2019a) Substantial emission reductions from Chinese power plants after the introduction of ultra-low emissions standards. Nat Energy 4(11):929–938. https://doi.org/10.1038/s41560-019-0468-1

Tang M, Huang X, Peng Y, Lu S (2020) Hierarchical porous carbon as a highly efficient adsorbent for toluene and benzene. Fuel 270:117478. https://doi.org/10.1016/j.fuel.2020.117478

Tang Y, Tao Y, Zhou T, Yang B, Wang Q, Zhu Z, Xie A, Luo S, Yao C, Li X (2019b) Direct Z-scheme La1-xCexMnO3 catalyst for photothermal degradation of toluene. Environ Sci Pollut Res 26(36):36832–36844. https://doi.org/10.1007/s11356-019-06856-7

Wang H, Guo H, Zhao Y, Dong X, Gong M (2020) Thermodynamic analysis of a petroleum volatile organic compounds (VOCs) condensation recovery system combined with mixed-refrigerant refrigeration. Int J Refrig 116:23–35. https://doi.org/10.1016/j.ijrefrig.2020.03.011

Wu Y, Xu Z, Liu S, Tang M, Lu S (2021) Emission characteristics of PM2.5 and components of condensable particulate matter from coal-fired industrial plants. Sci Total Environ 796:148782. https://doi.org/10.1016/j.scitotenv.2021.148782

Wu Y, Xu Z, Liu S, Tang, M, Lu S (2021b) Migration and emission characteristics of N-alkanes and phthalates in condensable particulate matter from coal-fired sources. *J Clean Prod 305*. https://doi.org/10.1016/j.jclepro.2021.127203

Xi Y, Wang Y, Yang D, Zhang Z, Liu W, Li Q, Qiu X (2019) K2CO3 activation enhancing the graphitization of porous lignin carbon derived from enzymatic hydrolysis lignin for high performance lithium-ion storage. J Alloys Compd 785:706–714. https://doi.org/10.1016/j.jallcom.2019.01.039

Xu J, Zhuo J, Yao Q (2019) Research progress on formation, emission characteristics and sampling methods of organic compounds from

coal combustion. Huagong Xuebao/CIESC J 70(8):2823–2834. https://doi.org/10.11949/0438-1157.20190287

Yang Y, Sun C, Lin B, Huang Q (2020) Surface modified and activated waste bone char for rapid and efficient VOCs adsorption. Chemosphere 256:127054. https://doi.org/10.1016/j.chemosphere.2020.127054

Zhang J, Shao J, Huang D, Feng Y, Zhang X, Zhang S, Chen H (2020) Influence of different precursors on the characteristic of nitrogen-enriched biochar and SO2 adsorption properties. *Chem Eng J 385*. https://doi.org/10.1016/j.cej.2019.123932

Zhang X, Gao B, Creamer AE, Cao C, Li Y (2017) Adsorption of VOCs onto engineered carbon materials: a review. J Hazard Mater 338:102–123. https://doi.org/10.1016/j.jhazmat.2017.05.013

Zhao X, Li X, Zhu T, Tang X (2018) Adsorption behavior of chloroform, carbon disulfide, and acetone on coconut shell-derived carbon: experimental investigation, simulation, and model study. Environ Sci Pollut Res 25(31):31219–31229. https://doi.org/10.1007/s11356-018-3103-y

Zhou D, Wei R, Zhu Y, Long H, Huang B, Wang Y, Wu S (2021) Calcium sulfate whisker one-step preparation using semi-dry flue gas desulfurization ash and directional growth control. J Clean Prod 290:125754. https://doi.org/10.1016/j.jclepro.2020.125754

Zhou T, Xie A, Wang Q, Li X, Zhu Z, Zhang W, Tao Y, Luo S (2020) A novel high-performance CeO2-CuMn2O4 catalyst for toluene degradation. Environ Sci Pollut Res 27(34):43150–43162. https://doi.org/10.1007/s11356-020-10190-8

Zhu Y, Gao J, Li Y, Sun F, Gao J, Wu S, Qin Y (2012) Preparation of activated carbons for SO2 adsorption by CO2 and steam activation. J Taiwan Inst Chem Eng 43(1):112–119. https://doi.org/10.1016/j.jtice.2011.06.009

Zubbri NA, Mohamed AR, Kamiuchi N, Mohammadi M (2020) Enhancement of CO2 adsorption on biochar sorbent modified by metal incorporation. Environ Sci Pollut Res 27(11):11809–11829. https://doi.org/10.1007/s11356-020-07734-3